Long-Wave Runup on a Sloping Beach, Validation of a Lagrangian Numerical Model

By

Louis-Alexandre Couston

A thesis submitted in partial satisfaction of the

requirements for the degree of

Master of Science

in

Engineering - Mechanical Engineering

in the

Graduate Division

of the

University of California, Berkeley

Committee in charge:

Professor M. Reza Alam, Chair
Professor Ronald W. Yeung
Professor Philip Marcus

Spring 2013

Abstract

Long-Wave Runup on a Sloping Beach,
Validation of a Lagrangian Numerical Model

by

Louis-Alexandre Couston

Master of Science in Engineering - Mechanical Engineering

University of California, Berkeley

Professor M. Reza Alam, Chair

We study the runup of two- and three-dimensional long-waves. The governing equations are derived in the Lagrangian framework and allow the analysis of non-breaking shallow-water waves propagating above an arbitrary seafloor. Nonlinearity is included but the flow is assumed to be incompressible, irrotational in vertical planes, and inviscid. Our analysis is purely numerical and based on explicit finite-difference methods. Our scheme is validated against analytical solutions of long-waves running up along a constant-slope seabed. Very good agreements are shown between our simulations and published predictions for both two- and three-dimensional cases. The model is highly flexible and computations of all presented results were a matter of minutes on a standard computer. The simplicity of this numerical implementation will allow us to investigate in the future many practical applications such as tsunami mitigation.

To Maminou. To my family.

Contents

List of Figures

List of Tables

Acknowledgments

I am indebted to my research advisor Professor Mohammad-Reza Alam, whose knowledge, stimulating suggestions, encouragement and availability made the past few months exciting. I would also like to thank Professor Ronald W. Yeung who gave me the opportunity to pursue a MS/PhD in Ocean Engineering here at UC Berkeley. Finally, I gratefully acknowledge all my committee members for the time they spent on this report and the constructive comments that followed. The present work was partially supported by the generous support of a Jaehne Graduate Scholarship.

1 Introduction

Harvesting marine energy, protecting offshore structures, coastal areas, seaports and bridges rely on ocean engineers. The modeling of water waves is very challenging as many complex processes take place at the same time. Hopefully, the propagation of water waves is quite different depending on parameters such as the shallowness or the Ursell number [1] and approximations can be made.

Researchers have always extensively studied long-waves because of their high destructive and energetic potential. A precise understanding of their dynamics would undoubtedly benefit many practical applications. For instance, wave-energy extractors need to be tuned for long-waves because they are the most predictable waves in the ocean, and coastal communities constantly need better protections against tsunamis, a specific kind of long-waves.

The long-wave assumption, also called shallow-water assumption, is well understood and greatly simplifies the general equations of motion of water-waves. Incompressibility of the ocean is also usually assumed, but irrotationality and linearity are simplifications that are not always appropriate. Therefore, it is of utmost importance for a researcher in ocean engineering to precisely state all assumptions and supporting claims.

The flow field can always be described in the Eulerian or Lagrangian framework, but it remains exceptional to derive the wave equations in the latter. Indeed, potential theory, developed in the Eulerian frame of reference, has been the most extensively used technique to predict the dynamics of ships and the ocean. Thus, in 1969, Wehausen was probably the first to introduce the Lagrangian coordinates in the analysis of ship hydrodynamics [2]. Later, in 1976, Higgins-Longuet and Cokelet [3] used a hybrid technique and took advantage of the Lagrangian concepts and equations to simulate the breaking of deep-water waves. This unique work has been emphasized by Yeung [4] in connection with other more popular Eulerian methods that he reviewed. More specifically, the Eulerian framework is not really adapted to study the runup of nonbreaking long-waves as the shoreline may move over large distances. Nevertheless, the superiority of the Lagrangian approach has not been proved and the runup phenomenon is still mainly studied in the Eulerian frame of reference.

In this thesis, the Lagrangian framework is used to derive the equations governing the dynamics of long-waves. The mathematical formulation is based on the incompressibility, irrotationality, inviscid and long-wave assumptions. The computational method is tested against different Lagrangian and Eulerian analytical results. In particular, the linear analytical two-dimensional runup/drawdown predicted by Shuto [5] and obtained numerically by Fujima [6] is observed for a uniform sloping beach. The two-dimensional nonlinear effect is then validated against the analytical solutions derived by Carrier et al. in 2003 [7]. Finally,

the linear three-dimensional formulation and its numerical implementation are validated against the solution derived by Sammarco and Renzi [8], who have analytically investigated the propagation of long-waves generated by a partially submerged landslide.

Despite the early developments of the linear Lagrangian theory by Shuto [5], the Eulerian approach has notably dominated the field in the last 50 years. Carrier and Greenspan's hodograph transformation paved the way for this predominant enthusiasm as they were able to derive an analytical solution for the fully nonlinear runup of long-waves over a uniformly sloping beach [7]. However, the complexity of the transformation made it impossible to generalize their results to any initial waveform and only a few practical applications of their discovery have been reported in the literature, as Carrier mentions it in a subsequent paper [9]. Carrier et al. [7], Synolakis [10] and Tadepalli and Synolakis [11] among others insisted on finding analytical solutions for the runup prediction of two-dimensional long-waves. Their works are inspiring but suffer from restrictive assumptions. Consequently, it is commonly acknowledged that numerical simulations are to take our understanding of this phenomenon a step further. Numerical efforts have slowly started. Shuto and Goto [12] were probably pioneers when they published their numerical results in 1978, but many recent works in the Eulerian framework from Lynett and Liu [13], Liu, Lynett and Synolakis [14] and Lynett and Liu [15] prove that the focus is now on what numerical simulations can help us understand.

The objective of this paper is dual. First, we derive the nonlinear three-dimensional equations of long-waves in a Lagrangian framework. Second, we present a numerical scheme and its validation against published analytical results. Beyond the scope of this thesis, we hope to have designed a numerical procedure that will allow a versatile and time-efficient investigation of many practical applications in the near future.

2 Mathematical formulation

We begin the mathematical analysis[1] by considering the two well accepted conservation of mass and linear momentum laws. The resulting equations are valid anywhere in the fluid but are very complicated. Consequently, we take advantage of various assumptions and boundary conditions to derive the three-dimensional and two-dimensional set of reduced equations for the free surface only, i.e. (32), (33), (34), (35), and (36).

2.1 General three-dimensional governing equations

2.1.1 Initial and referent configurations

When we work in a Lagrangian frame of reference we have to choose a referent configuration from which we will derive our governing equations. Two options are available. One option is to choose the referent situation so that it matches the initial value problem being tried, i.e. we consider the initial wave profile (e.g. a Gaussian wave) and draw a Cartesian grid that defines where the fluid particles are at the starting time of the simulation. This procedure makes it really easy to obtain the Lagrangian equivalent of any Eulerian initial profile. However, the derivation of the governing equations is somehow more mathematically involved and thus makes the numerical implementation more demanding. For that matter, we chose the referent situation to be the flat free surface. This method forces us to spend some time transferring the Eulerian initial values to our Lagrangian framework but benefits every other aspect.

2.1.2 Mass and momentum conservation laws

We define the flat free surface on top of a calm ocean as our referent configuration. The Cartesian coordinates system (a, b, c) is used as a means to identify the referent position of all particles being followed over time. That is, if $\underline{P}$ denotes the particles' location such that $\underline{P}_{ref} = (x_{ref}, y_{ref}, z_{ref}) = (a, b, c)$; $\underline{P}(t) = (x(a, b, c, t), y(a, b, c, t), z(a, b, c, t))$ is the instantaneous location of all particles at any time.

Mass conservation in a Lagrangian framework. As can be seen in figure (1), the particle $\underline{P}$ moves with time, and its associated volume of fluid defined in the referent configuration by a cube with volume $\mathcal{V}_{ref}$ can be a priori transformed in any parallelepiped of volume $\mathcal{V}(t)$. However, as we assume the fluid to be incompressible, we have to force our element's volume to remain constant

[1] This section follows to some extent the earlier works of Shuto [5] and Fujima [6].

over time, ie. $\mathcal{V}_{ref} = \mathcal{V}(t)\ \forall t$. Since the amount of stretching of a cube in all three directions is given by the transformation matrix $\underline{\underline{F}}$, the continuity equation is satisfied when

$$J(t) = \det(\underline{\underline{F}}(t)) = \det \begin{pmatrix} x_a & x_b & x_c \\ y_a & y_b & y_c \\ z_a & z_b & z_c \end{pmatrix} = \begin{vmatrix} x_a & x_b & x_c \\ y_a & y_b & y_c \\ z_a & z_b & z_c \end{vmatrix} = 1 \tag{1}$$

where $J(t)$ is the Jacobian of the transformation matrix $\underline{\underline{F}}(t)$ such that (see figure (1)):

$$\underline{dP}(t) = \underline{\underline{F}}(t).\underline{dP}_{ref}$$

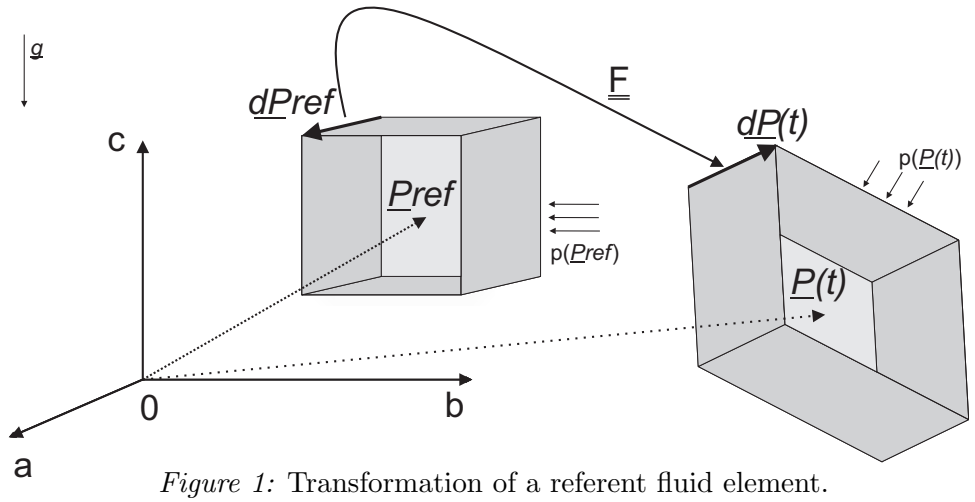

Figure 1: Transformation of a referent fluid element.

Linear momentum conservation in a Lagrangian framework. Looking again at figure (1), one can imagine that in an inviscid fluid dominated by the pressure and gravity forces, the conservation of linear momentum simply reads

$$\frac{d}{dt}\int_{\mathcal{V}(t)} \rho \underline{U} dV = \int_{\mathcal{V}(t)} \underline{f}_B(\underline{P}(t), t) dV + \int_{\partial\mathcal{V}(t)} \underline{\underline{\sigma}}(\underline{P}(t), t).\underline{n} dS \tag{2}$$

where the integration is performed over the new fluid element's volume $\mathcal{V}(t)$ or associated surface and the stress tensor is linearly proportional to the pressure distribution in the fluid, i.e. $\underline{\underline{\sigma}}(\underline{P}(t), t) = -p(\underline{P}(t), t)\underline{\underline{I}}$. We recall that we use the notations $\underline{P}(t)$ and $\underline{P}_{ref} = (a, b, c)$ for the instantaneous and referent locations of all particles and:

$$\underline{P}(t) = (x(\underline{P}_{ref}, t), y(\underline{P}_{ref}, t), z(\underline{P}_{ref}, t)),\ \ \underline{U} = \begin{pmatrix} x_t(\underline{P}_{ref}, t) \\ y_t(\underline{P}_{ref}, t) \\ z_t(\underline{P}_{ref}, t) \end{pmatrix}$$

It has to be noted that $\underline{U}$ can be seen as the Lagrangian velocity of the referent fluid particle $\underline{P}_{ref}$ at time t, or as the Eulerian velocity of the particle that would be at point $\underline{P}(t)$ at time t. The integrals in equation (2) are substituted by new integrals as we switch from the instantaneous coordinates system $(x(a,b,c,t), y(a,b,c,t), z(a,b,c,t))$ to the referent coordinates system (a,b,c). Hence, (2) becomes

$$\frac{d}{dt}\int_{\mathcal{V}_{ref}} \rho \underline{U}(\underline{P}_{ref},t) J dV_{ref} = \int_{\mathcal{V}_{ref}} \left[\rho \underline{g} - \underline{\underline{F}}^{-1} \nabla_{(a,b,c)} p(\underline{P}_{ref},t)\right] J dV_{ref} \tag{3}$$

where $J(t) = 1$ is the Jacobian of the transformation matrix. The coordinate c and variable $z(a,b,c)$ are conveniently chosen positive in the opposite direction of gravity, and (3) being valid for any referent volume we get:

$$\begin{pmatrix} x_{tt}(a,b,c,t) \\ y_{tt}(a,b,c,t) \\ z_{tt}(a,b,c,t) + g \end{pmatrix} = -\frac{1}{\rho} \begin{pmatrix} x_a & x_b & x_c \\ y_a & y_b & y_c \\ z_a & z_b & z_c \end{pmatrix}^{-1} \begin{pmatrix} p_a \\ p_b \\ p_c \end{pmatrix} \tag{4}$$

Finally, by taking advantage of (1) and rearranging (4), we obtain the dimensional equations governing the motion of a three-dimensional fluid

$$x_{tt} + \frac{1}{\rho}\frac{\partial(p,y,z)}{\partial(a,b,c)} = 0 \tag{5}$$

$$y_{tt} + \frac{1}{\rho}\frac{\partial(x,p,z)}{\partial(a,b,c)} = 0 \tag{6}$$

$$z_{tt} + g + \frac{1}{\rho}\frac{\partial(x,y,p)}{\partial(a,b,c)} = 0 \tag{7}$$

where (x,y,z,p) are functions of (a,b,c).

2.2 Boundary conditions and assumptions

In this section we first introduce what we can learn from the boundary conditions. We then present all assumptions and the resulting simplifications in the governing equations. The incompressibility and inviscid flow conditions have already been enforced, so only the irrotationality and long-waves assumptions are actually introduced. Finally, we accomodate the equations to have them govern the displacement variables' evolution in lieu of the absolute position.

2.2.1 Boundary conditions

Free surface conditions. As we are interested in the free surface of the ocean, we will write all governing equations in the particular case of $c = 0$. We assume that if a particle is on the free surface it will stay on it its entire lifespan, i.e. if η denotes the Eulerian free surface elevation, the kinematic boundary conditions is:

$$z(a, b, c = 0, t) = \eta(x, y, t), \forall a, b, t \tag{8}$$

The dynamic boundary condition simply states that the pressure on the free surface is that of the ambient air

$$p(a, b, c = 0, t) = p_{air} \tag{9}$$

where p_{air} denotes the atmospheric pressure and is casually assumed to be zero. This condition also implies

$$\nabla_{(a,b)} p(a, b, c = 0, t) = 0 \tag{10}$$

where $\nabla_{(a,b)}$ is the two-dimensional gradient operator in terms of the Lagrangian horizontal coordinates in the referent configuration.

Seabed conditions. We suppose that if a particle is initially resting on the ocean floor it will stay on it. In other words, its degree of freedom is reduced to two and

$$z(a, b, c = -h(a, b, 0), t) = -h(x, y, t), \forall a, b, t \tag{11}$$

where $h(x, y, t)$ is the water depth function such that its opposite describes the seabed plane at any time. The reader should realize at this point that the free surface elevation and the water depth are naturally given in terms of Eulerian coordinates although the analysis is conducted in the Lagrangian frame of reference.

2.2.2 Irrotationality assumption

We assume that the fluid is irrotational in any vertical plane to further simplify our equations. Let us consider one more time the volume of fluid associated with an arbitrary particle. The element is not rotating if and only if its diagonals' directions are unchanged over time. This idea is illustrated in the following figure for a $x - z$ plane and requires

$$\alpha = \gamma \Leftrightarrow \frac{z_a}{x_a} = \frac{x_c}{z_c} \Leftrightarrow x_a x_c = z_a z_c \tag{12}$$

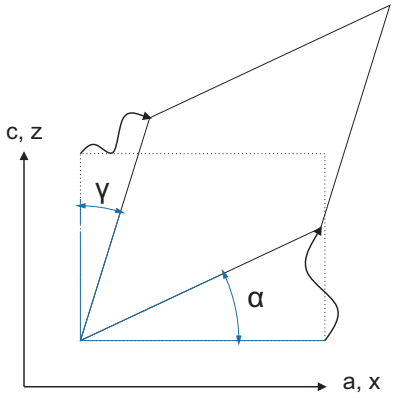

Figure 2: Illustration of the irrotationality condition.

Similarly for a $y - z$ plane, we have

$$\frac{z_b}{y_b} = \frac{y_c}{z_c} \Leftrightarrow y_b y_c = z_b z_c \tag{13}$$

This simplification has already been used by Fujima [6] and, as he pointed out, is justified by the fact that we consider the fluid to be inviscid.

2.2.3 Scaling and long-wave assumption

The horizontal and vertical scales of long-waves are vastly different. That's why the non-dimensionalization of our physical quantities relies on two different lengths. The horizontal variables and coordinates are scaled by the length L:

$$a \leftarrow \widetilde{a}L \quad b \leftarrow \widetilde{b}L \quad x \leftarrow \widetilde{x}L \quad y \leftarrow \widetilde{y}L$$

The vertical quantities are scaled by H:

$$c \leftarrow \widetilde{c}H \quad z \leftarrow \widetilde{z}H \quad \eta \leftarrow \widetilde{\eta}H \quad h \leftarrow \widetilde{h}H$$

And the time and pressure variables become:

$$t \leftarrow \widetilde{t}\frac{L}{\sqrt{gH}} \quad p \leftarrow \widetilde{p}\rho g H$$

where the wide tilde symbol denotes dimensionless variables. In general, L and H are estimates of the wavelength and mean water depth such that $\frac{H}{L} = \mu \ll 1$ is the shallowness parameter. However, if the nonlinearity parameter $\epsilon = \frac{A}{H}$ is of order unity with A and H the wave height and mean water depth, the approximate

wave height can also be picked as the vertical normalizing length[2]. It should also be noticed that if H is the mean water depth, the time variable is scaled by the linear long-wave phase velocity and the wavelength.

2.3 Final three-dimensional governing equations

In this section, we derive the dimensionless equations that govern the three-dimensional free surface evolution of long-waves for an incompressible and irrotational flow. The final form is written in terms of the displacements' variables instead of the absolute locations.

2.3.1 Governing equations for the free surface

Simplifications following the long-wave assumption. The proposed scaling enables us to transform equations (1) (5) (6) and (7) into

$$\frac{\partial(x,y,z)}{\partial(a,b,c)} = 1 \tag{14}$$

$$x_{tt} + \frac{\partial(p,y,z)}{\partial(a,b,c)} = 0 \tag{15}$$

$$y_{tt} + \frac{\partial(x,p,z)}{\partial(a,b,c)} = 0 \tag{16}$$

$$\mu^2 z_{tt} + 1 + \frac{\partial(x,y,p)}{\partial(a,b,c)} = 0 \tag{17}$$

where the variables p, x, y, z and coordinates a, b, c are dimensionless and we will omit the wide tilde symbol from now on. The long-wave assumption $\frac{H}{L} = \mu \ll 1$ allows us to reduce (17) to:

$$1 + \frac{\partial(x,y,p)}{\partial(a,b,c)} = 0 \tag{18}$$

Similarly, the irrotationality conditions in their dimensionless forms can be rewritten as:

$$x_a x_c = \mu^2 z_a z_c \ll 1 \tag{19}$$

$$y_b y_c = \mu^2 z_b z_c \ll 1 \tag{20}$$

[2]Note that if $\epsilon \ll 1$ the wave height can still be chosen to scale the vertical variables and coordinates, although the dimensionless water depth won't be of order unity anymore.

To the leading order in μ these two equations have a right-hand-side equal to zero. Since it would not be physical to have $x_a = 0$ nor $y_b = 0$, we necessarily have:

$$x_c = y_c = 0 \tag{21}$$

Consequently, the distribution of the horizontal velocity is uniform vertically, and any infinitely thin vertical cuboid of fluid remains a cuboid over time.

Simplifications following the irrotationality assumption. As a consequence of (21), the continuity equation (14) takes the following form

$$\begin{vmatrix} x_a & x_b & x_c \\ y_a & y_b & y_c \\ z_a & z_b & z_c \end{vmatrix} = \begin{vmatrix} x_a & x_b & 0 \\ y_a & y_b & 0 \\ z_a & z_b & z_c \end{vmatrix} = z_c \begin{vmatrix} x_a & x_b \\ y_a & y_b \end{vmatrix} = z_c s = 1 \tag{22}$$

where it has to be noticed that the determinant s of the $x - y$ transformation matrix is a function of a, b, t only. Similarly, the momentum equation in the z-direction (18) becomes:

$$p_c = -\frac{1}{s} \tag{23}$$

This last equation shows that the pressure gradient in the vertical direction is purely hydrostatic.

Application of the boundary conditions. Here we derive the $x-y$ governing equations for the free surface by taking advantage of the boundary conditions. In fact, using the dynamic free surface boundary condition (10) and the simplified momentum equation in the z-direction (23), equations (15) and (16) become

$$x_{tt} = \frac{1}{s} \begin{vmatrix} y_a & y_b \\ z_a & z_b \end{vmatrix} \tag{24}$$

$$y_{tt} = -\frac{1}{s} \begin{vmatrix} x_a & x_b \\ z_a & z_b \end{vmatrix} \tag{25}$$

where we recall that s is the determinant of the $x - y$ transformation matrix. Finally, the vertical integration of the continuity equation (22) gives the dimensionless free surface elevation, i.e.

$$z(a, b, 0, t) - z(a, b, -h(a, b, t)) = \int_{-h(a,b,0)}^{0} z_c dc = \frac{h(a, b, 0)}{s}$$

or,

$$z(a, b, 0, t) = \frac{h(a, b, 0)}{s} - h(x, y, t) \tag{26}$$

as we used the seabed kinematic boundary conditions (11). We note that these equations only govern the evolution of the free surface and are independent of c. In addition, in (24) and (25) z can be easily substituted by x, y through (34). Thus, we started from three coupled equations for x, y, z valid $\forall a, b, c$ and derived a reduced system of two equations on x, y as functions of a, b only. This surprising simplification results from (21).

2.3.2 Displacement variables and linearization

The instantaneous location $\underline{P}(t) = (x, y, z)$ of any particle can always be decomposed in terms of its referent location $\underline{P}_{ref} = (a, b, c)$ and its displacement variables (X, Y, Z) such that:

$$\begin{aligned} x(a,b,c,t) &= a + X(a,b,c,t) \\ y(a,b,c,t) &= b + Y(a,b,c,t) \\ z(a,b,c,t) &= c + Z(a,b,c,t) \end{aligned} \tag{27}$$

It is really convenient to work with the displacement variables because the associated governing equations can be easily linearized. The first two dimensionless equations for X, Y, Z come from the linear-momentum conservation law, i.e. are derived from (24) (25) and (27):

$$X_{tt} = -\frac{1}{s}\left(Z_a - \begin{vmatrix} Y_a & Y_b \\ Z_a & Z_b \end{vmatrix}\right) \tag{28}$$

$$Y_{tt} = -\frac{1}{s}\left(Z_b + \begin{vmatrix} X_a & X_b \\ Z_a & Z_b \end{vmatrix}\right) \tag{29}$$

And the third dimensionless equation for X, Y, Z expresses mass conservation, i.e. is derived from (26) and (27)

$$Z(a,b,0,t) = \frac{h(a,b,t_0)}{s} - h(X+a, Y+b, t) \tag{30}$$

where

$$s = 1 + X_a + Y_b + \begin{vmatrix} X_a & X_b \\ Y_a & Y_b \end{vmatrix} = 1 + X_a + Y_b + S \tag{31}$$

These are the nonlinear shallow-water waves equations, which govern the free surface evolution of an incompressible, inviscid and irrotational fluid in terms of the displacement variables. They are valid for $c = 0$, and we recall that X, Y, Z are functions of a, b, t and represent the two horizontal and one vertical displacements of any particle that was on the free surface in the referent configuration. The linear form of the last three equations assuming that X, Y, Z and all their derivatives are really small compared to one is:

$$X_{tt} = -Z_a \tag{32}$$

$$Y_{tt} = -Z_b \tag{33}$$

$$Z(a,b,0,t) = h(a,b,t_0)(1 - X_a - Y_b) - h(X + a, Y + b, t) \tag{34}$$

2.4 Two-dimensional governing equations

The reduced one horizontal dimension governing equations can help understand a few concepts that would be too hard to solve analytically or numerically for two horizontal dimensions. Moreover, very few three-dimensional studies have been published as noted just a few years ago by Lynett and Liu [15] and Sammarco and Renzi [8]. Hence we first require our code to be validated against two-dimensional results. In that respect, the two-dimensional form of the dimensionless equations (28) (29) and (30) is derived and further simplified for two simple bathymetries.

We start from (28) and (30) and drop all b, y related terms, i.e.

$$X_{tt} = -\frac{Z_a}{1 + X_a} \tag{35}$$

$$Z(a,0,t) = \frac{h(a,t_0)}{1 + X_a} - h(X + a, t) \tag{36}$$

If the dimensionless water depth is constant and equal to h, the free surface is governed by a set of two equations that is:

$$X_{tt} = h\frac{X_{aa}}{(1 + X_a)^3}$$

$$Z = -h\frac{X_a}{1 + X_a} \tag{37}$$

The linear form of which is:

$$X_{tt} = hX_{aa}$$

$$Z = -hX_a \tag{38}$$

This last set of equations dictates the propagation of shallow-water waves over a constant seabed. Note that we used the continuity equation to substitute Z in terms of X such that only one partial differential equation on X has to be solved to get the free surface displacement. A particular solution based on sine and cosine functions can be derived. Interesting insights can be found in Fujima's work [6] and Shuto's paper [5]. Fundamentally, a Lagrangian linear solution already includes what we would see as Eulerian nonlinearity as both the vertical

and horizontal displacement are adjusted in time.

If the slope of the dimensionless water depth is constant and equal to β, the new set of equations that governs the two-dimensional free surface evolution is:

$$X_{tt} = -\frac{\beta}{(1+X_a)}\left[\frac{1}{1+X_a} - \frac{aX_{aa}}{(1+X_a)^2} - (1+X_a)\right]$$

$$Z = \frac{\beta a}{1+X_a} - \beta(a+X) \tag{39}$$

The linear form of which is:

$$X_{tt} = \beta\left(aX_{aa} + 2X_a\right)$$

$$Z = -\beta(aX_a + X) \tag{40}$$

If α is the slope of the dimensional water depth function, $H = L\alpha$ is a vertical scaling that makes $\beta = 1$, and the evolution of the dimensionless variables following (39) (40) is independent of β. Note that this scaling is legitimate if and only if the slope is really mild such that $\mu = \frac{H}{L} = \alpha \ll 1$ is true. Analytical solutions also exist in this case. The full derivation can be found in Shuto [5], but we will only consider the solution that is most physical or which does not blow up as its arguments tend to zero. A thorough discussion on this topic follows in the next section as our numerical scheme is tested against this linear solution.

3 Numerical model for two-dimensional waves and validations

By the end of this part we hope to give the reader all the necessary tools to numerically solve the partial differential equations derived in the previous section. Different numerical schemes are available and have been used to simulate the wave equation in a Lagrangian frame of reference. For instance, Zelt [16] used a finite-element method to investigate the runup of nonbreaking and breaking solitary waves whereas Shuto and Goto [12] used a finite-difference technique. We decided to implement the latter method because of its simplicity.

We use a fixed collocated grid which corresponds to a totally calm sea state, i.e. the horizontal and vertical displacements are zero in the referent situation. We use the explicit 4^{th} order scheme of Runge-Kutta for time integration and a basic central finite difference technique of 2^{nd} order to get the spatial derivatives. The method is developed for the nonlinear equations and we assume that the reader could easily implement the linear equivalent. The discretization is performed on the dimensionless equations, i.e. (35) and (36) governing the runup of two-dimensional waves on a uniformly sloping beach.

We point out the fact that all existing analytical results suffer from really strong restrictions. For instance, Carrier and Greenspan's Eulerian derivation [7] and Shuto Lagrangian developments [5] assume a constant-slope seabed. Shuto's analytical solution lacks the nonlinear effect taken into account by Carrier et al., but the latter proposed a transformation so complex that the theoretical runup was obtained only for four very specific initial value problems. Fundamentally, all existing analytical solutions are worth comparing to, but future insights on the propagation and runup/rundown of long-waves on and along the coasts will be claimed by numerical experiments.

Our mathematical formulation and numerical model both include nonlinearity and suffer no restriction on the water-depth function. However, we take advantage of the latter versatility exclusively in our three-dimensional simulations as we investigate the propagation of tsunamis generated by a landslide.

3.1 Nearshore unboundedness

It has been observed in early simulations that rapidly-growing oscillations are likely to occur nearshore. No refined spatial grids nor smaller time steps could make it any better. It seems that the simulation is subject to growing non-physical solutions even though the scheme satisfies an equivalent Courant-Friedrichs-Lewy condition (CFL). In the worst case scenario the numerical solution blows up though we did not expected it to. This may partly explain the nonexistence of a predom-

inant code on the subject of long-waves runup in a Lagrangian framework.
As proved by Shuto [5], diverging functions for zero arguments, i.e. nearshore, satisfy the two-dimensional governing equations in the case of a constant-slope seabed. In its derivation, Nobuo Shuto assumed that the separation of space and time variables was acceptable, and found that the spatial dependency of the vertical displacement could be either a zero order Weber or Bessel function. The Weber functions are also called Bessel function of second kind and have the property to diverge for zero arguments.
Thus, we expect the full solution of the general two- and three-dimensional governing equations to have a diverging term similar to the Weber functions. The initial value problems at hands do not include such unbounded functions, but the numerical integration of the solution at each time step is likely to produce nearshore errors as the horizontal acceleration is inversely proportional to $1-\epsilon$, where ϵ is the nonlinearity parameter (see Zelt and Raichlen [17]). Therefore, a technique could be to use at each time step the Hankel transform with a finite number of modes to decompose the numerical solution as a series of weighted Bessel functions of the first kind. The possible small discontinuity of the nearshore free surface elevation would be neglected in this decomposition given the fact that only a few number of modes are selected. Next, the inverse Hankel transform could be applied to get a well-behaved approximation of the initial free surface solution. The downsides of this approach are the computational cost of the Hankel and inverse Hankel transforms and the complexity of the finite series approximation. Hence we developed a second method, which is to dispose of the onshore node. This technique requires no additional maths nor operations yet yield successful results. Specifically, the computational domain is a set of referent free surface particles, which supposedly starts with the particle on the shore (i.e. at the wet/dry interface) and ends at the offshore boundary. However, since the unboundedness of the solution is likely to start nearshore, we do not update/work with the shore particle. The distance between the first node of our grid and the onshore particle will be referred to as the staggering parameter in subsequent sections and is typically of the order of the spatial resolution.

3.2 Numerical procedure

As said in the introduction, two-dimensional simulations were primarily run to validate the mathematical formulation and the numerical scheme against well accepted results. The extensive numerical experiments that were conducted also helped us formulate the technique to bypass the existence of diverging modes as solutions of the governing equations. The numerical formulation is based on an explicit Runge-Kutta and central finite-difference technique to respectively integrate in time the solutions and get their associated spatial derivatives. In this section,

we will first exhibit the basic structures of our two-dimensional code. Then, the two-dimensional experiments run for validation will be presented.

3.2.1 Basic structure of the algorithm

The code initially calls an external function that returns the initial values of the horizontal and vertical displacements and velocities over all nodes defining the spatial grid. Depending on the spatial steps another external function gives a discrete time vector satisfying an equivalent CFL condition. The code is then free to run as long as necessary and calls different nested and external functions to get the spatial derivatives and integrate in time the solution.

3.2.2 Grids construction

The simulation of two-dimensional surface waves is actually based on the time update of a single dimension curve whose evolution is both horizontal and vertical, hence two-dimensional. Because the referent configuration is the calm free surface, the instantaneous locations of all particles that constitute the air-ocean interface is a function of the referent horizontal location and time only. Therefore, we use the set of coordinates $a_j,\ j \in \mathbb{N}^*$ as the horizontal locations of our l_a particles in the referent configuration, and the vertical position $c_j = 0$ is simply omitted. We assume that the runup motion over the dry land always occurs on the left-hand-side of the domain. The particles in the referent configuration can be uniformly, or non uniformly distributed. If the a_j^u (resp. a_j^{nu}) with $j \in [1, l_a]$ are the uniformly (resp. non uniformly) spaced particles, we note $F_{m,\delta}$ the quadratic function such that

$$a_j^{nu} = F_{m,\delta}(a_j^u) = \frac{1-m}{a_{l_a} - \delta}(a_j^u - \delta)^2 + m(a_j^u - \delta) + \delta \tag{41}$$

where, $m \in [0; 1]$ is the uniformity parameter, ie. $m = 0$ means that we have a highly non-uniform grid and $m = 1$ means that the grid is strictly uniform. In (41), δ is our previously defined staggering parameter and allows us to have the first grid particle slightly away from the shore (figure (3)). All displacements variables are updated over time on the grid points and the exact shore runup can be obtained using a polynomial interpolation of $X(0, t)$ at any time.

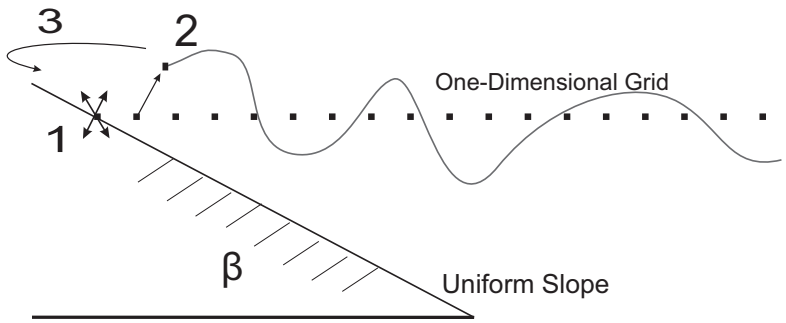

Figure 3: This is the geometry of our two-dimensional problems. The sloping beach is always assumed to be on the left-hand-side of the domain whereas the right-hand-side is an open boundary. β is the dimensionless slope. (1) The particle on the shoreline is removed from the computational grid. (2) The X, Z displacements of the first node (i.e. δ away from the shore in the referent configuration) are tracked over time. (3) A polynomial interpolation is required to get a more accurate runup.

Once the spatial grid is defined, the uniform time span can be obtained using an equivalent Courant-Friedrichs-Lewy condition to find the largest time step that theoretically allows numerical stability. We do the stability analysis for equations (40) and find

$$\Delta t \ll \min\{\frac{\Delta a}{\sqrt{\beta a}}, \frac{\sqrt{\Delta a}}{\sqrt{\beta}}\} \tag{42}$$

where Δa and β are the minimum spatial step and mean seabed slope respectively.

3.2.3 Initial and boundary value problem

The physical phenomena we plan to address are referred to as initial, boundary or mixed value problems. If the initial water surface is not calm, i.e. the initial vertical displacements are non zero, the starting vertical and horizontal displacements have to be carefully taken care of. As said in preceding sections, we decided to derive the governing equations for a referent still water configuration. Consequently, a non zero initial profile should be considered as the result of a virtual horizontal and vertical transformation of the initially at rest free surface. From a practical standpoint, if $\eta(x)$ describes the initial free surface, we can get $X(a, 0)$ from the continuity equation as

$$\eta(x, 0) = \eta(a + X(a, 0), 0) = Z(a, 0) = \frac{h(a, 0)}{1 + X_a(a, 0)} - h(a + X(a, 0), 0) \tag{43}$$

The equation for $X(a, 0)$ is a nonlinear 1^{st} order ODE which can be solved using a finite-difference scheme. The boundary condition $X(0, 0) = 0$ is a convenient boundary condition if appropriate.

Although no boundary value problem is presented in this work, it is worth highlighting a few points. As already mentioned, the left-hand-side of the domain is assumed to be the dry land region, and we have a free boundary condition for the horizontal displacement. The vertical motion is obtained as we expect that the particle in contact with the shore should always stay on the shore. However, since we do not update this particle, the vertical position of our first node is actually found through the continuity equation. A numerical experiment is said to be a boundary value problem if the farthest offshore point's motion is forced. In such cases, the numerical update should incorporate this forcing. If no forcing is prescribed, the right-hand-side should be an open boundary. However, no technique can be easily implemented and quite often reflections come from the right. Thus, the domain should be big enough so that these reflections do not perturb what is being observed at the shoreline.

3.2.4 Horizontal and vertical displacement update

Let's now consider that X and X_t are known at time t. The time integration of the governing equation is based on the finite difference method developed by Runge Kutta with accuracy $O(\Delta t^4)$ if Δt is the time step. In order to get $X_{tt}(a_j, t), j \in \mathbb{N}^*$, hence $X_t(a_j, t + \Delta t)$ and $X(a_j, t + 2\Delta t)$, we need to numerically assess the value of $X_{a,j}$ and $X_{aa,j}$. If $\mathfrak{D}$ represents a discrete 1^{st} order differential operator, and $\mathfrak{D}_2$ is its 2^{nd} order equivalent, we have

$$X_{tt,j} = \frac{-1}{1 + X_{a,j}} \left[\frac{h_a(a_j, t)}{1 + X_{a,j}} - \frac{h(a_j, t) X_{aa,j}}{(1 + X_{a,j})^2} - h_x(x_j, t)(1 + X_{a,j}) \right] \tag{44}$$

Where $X_{a,j} = [\mathfrak{D}X]_j$, $X_{aa,j} = [\mathfrak{D}_2 X]_j$, $h_a(a_j, t) = [\mathfrak{D}h]_j$ and $h_x(x_j, t)$ needs a little bit more work since it is not evaluated on one of the referent nodes. It should be noted that this equation on X only is derived from the coupled $X - Z$ equations (35) and (36). The latter set of equations would be slightly easier to implement but would lack the information that a single equation on X, in lieu of two, is necessary to integrate to predict the runup at all times.

The update for the interior points using $\mathfrak{D}$ (resp. $\mathfrak{D}_2$) is straightforward. For instance, if we use a two stencil points technique (resp. three stencil points) over a uniform grid, the two linear operators are given by

$$[\mathfrak{D}]_{i,j} = \frac{1}{2\Delta a} \left(\delta_{i+1,j} - \delta_{i-1,j} \right) \tag{45}$$

$$[\mathfrak{D}_2]_{i,j} = \frac{1}{\Delta a^2} \left(\delta_{i+1,j} - 2\delta_{i,j} + \delta_{i-1,j} \right) \tag{46}$$

where Δa is the distance between each grid point. We cannot use a central finite-difference technique on the boundaries of our domain . Therefore, on the left-hand-side (resp. right-hand-side) we use a forward finite-difference (resp. backward finite-difference). This nearshore boundary condition is not exact and many other ideas (e.g. using ghost nodes) have been tried. Yet, none makes more physical sense than the others. Finally, the backward finite-difference doesn't allow outgoing waves. A careful implementation of the Sommerfeld radiation condition would probably work better but still need to be implemented. Another option would be to use a sponge layer technique, i.e. to add a progressive damping term in the governing equations of the say 10% farthest points from the shore.

3.3 Validation of the two-dimensional linear model

Our numerical model is first compared with the analytical solution obtained in a Lagrangian framework for the linear runup/rundown of water waves over a straight beach with slope α. The theory and all derivations can be found in Shuto's work [5]. The non-dimensionalization of our equations is performed using $L = 1m$ for all horizontal variables and $H = L\alpha$ for the vertical direction, thus making the dimensionless slope $\beta = 1$. Both linear and nonlinear numerical results are compared to the analytical solution. The effect of the staggering and uniformity parameters are discussed.

3.3.1 Lagrangian linear analytical solution

We only retain the non-diverging terms from the dimensional general solution found by Shuto [5], that is the one associated with the Bessel functions of the first kind and first order for the horizontal displacement. The solution obtained is a standing wave running up and down a uniform sloping beach.

$$Z(a,t) = -\mathcal{H} J_0\left(2\sigma\sqrt{\frac{a}{\alpha g}}\right) cos(\sigma t) \tag{47}$$

$$X(a,t) = \frac{\mathcal{H}}{\sigma}\sqrt{\frac{g}{\alpha a}} J_1\left(2\sigma\sqrt{\frac{a}{\alpha g}}\right) cos(\sigma t) \tag{48}$$

The dimensionless form of which is

$$Z(a,t) = -\widetilde{\mathcal{H}} J_0\left(2\widetilde{\sigma}\sqrt{a}\right) cos(\widetilde{\sigma} t) \tag{49}$$

$$X(a,t) = \frac{\widetilde{\mathcal{H}}}{\widetilde{\sigma}}\sqrt{a} J_1\left(2\widetilde{\sigma}\sqrt{a}\right) cos(\widetilde{\sigma} t) \tag{50}$$

where $\widetilde{\sigma}$ and $\widetilde{\mathcal{H}}$ are the dimensionless equivalent of σ and $\mathcal{H}$ appropriately scaled by H and $\sqrt{\frac{g\alpha}{L}}$. Note that the dimensionless variables X, Z are independent of the slope α.

3.3.2 Numerical simulations

In order to check whether our code is well behaved, we start off with an initial profile given by (49) and (50) at time $t = 0$. Note that this initial value problem is easy to implement because the variables are expressed in terms of the referent coordinates. The following figures show comparisons at different time of the dimensionless linear and nonlinear numerical simulations with the linear analytical solution (49) (50). The parameters are those of Koji Fujima [6] who did this comparison a few years earlier (i.e. $\alpha = \frac{1}{20}$, $\mathcal{H} = 20\ m$, $T = 300\ s$ such that $\widetilde{\mathcal{H}} = 1$ and $\widetilde{\sigma} = \frac{2\pi}{T}\sqrt{\frac{1}{g\alpha}} = 0.0299$). The simulations were run up to 500 seconds. The numerical integration converges to a fixed solution as the number of spatial nodes and time steps are increased. The numerical horizontal acceleration $X_{tt}(a = a(l_a), t)$ is analytically updated, i.e. using (48), to avoid discrepancies due to the offshore-boundary backward finite-difference approximation.

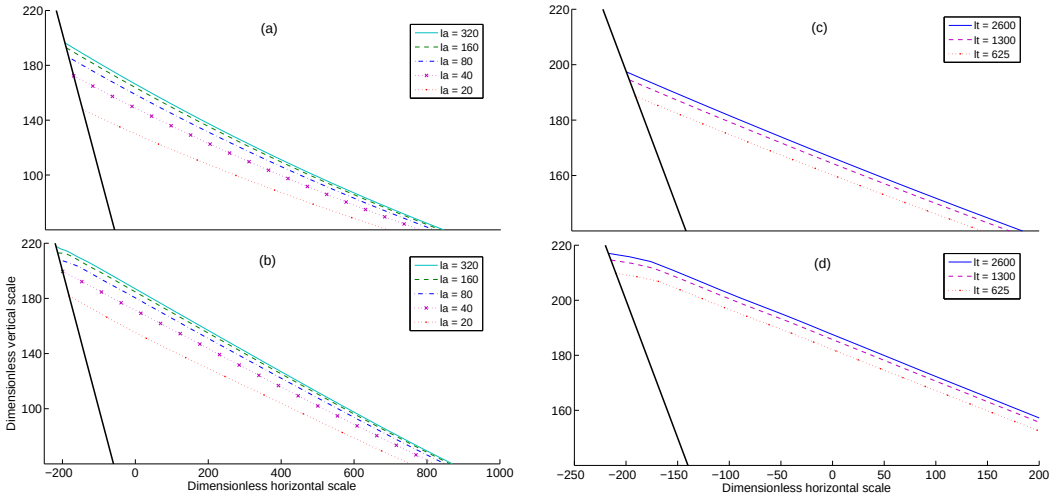

Figure 4: Spatial and time convergence of the linear and nonlinear schemes at time 400 seconds. The initial profile is given by the theory. Graphs on the left show the spatial convergence for a time/space grid size ratio of 125/20. Those on the right exhibit the time convergence for la = 100. The upper plots refer to the linear case, whereas the lower ones were obtained for nonlinear simulations. la is the grid size, lt the number of time steps.

3.3.3 Results and discussions

The separation of variables that allowed the derivation of the analytical solution is validated as the linear simulation closely follows the theoretical model. As

observed by Koji Fujima, the maximum runup/rundown can be quite satisfactorily approximated by the linear theory. The nonlinear effect has indeed little effect on the extreme values. However, the evolution is quite different between the linear and nonlinear simulations. The shoreward (resp. seaward) velocity increases much faster after reaching the maximum drawdown (resp. highest runup) point as we take into account the nonlinear effect. This change should be accounted for as for a nonuniform slope the extreme runup/rundown values might differ considerably.

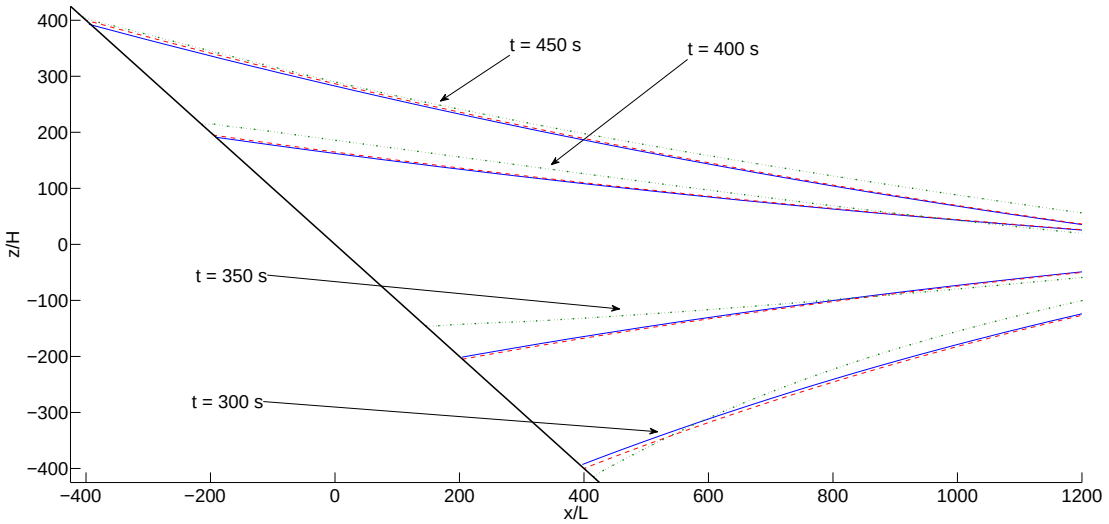

Figure 5: Snapshots at four different times of the linear and nonlinear numerical simulations along with the analytical solution that comes from the linear theory of long water-waves running up and down a constant slope seabed. The simulations were obtained for 100 spatial nodes and a total of 991 time steps were run to simulate a 500 seconds motion. The solid blue, dashed red, and dotted green with small markers lines represent the analytical, linear, and nonlinear simulated solutions.

3.4 Validation of the two-dimensional nonlinear model

3.4.1 Eulerian nonlinear analytical solutions

We turn to Kanoglu's work [18] and Carrier et al. [9] for the validation of the nonlinear case. They used a hodograph transformation, today known as Carrier-Greenspan, of the governing equations in the Eulerian frame of reference in order to find analytical solutions for the runup of long-waves. They theoretically obtained both maximum seaward and shoreward velocities and the maximum

runup/rundown for four different initial waveforms. We compare their results with ours in a table later in this paragraph.

3.4.2 Initial profiles

As said earlier,the referent situation being the flat surface, any non zero initial vertical profile requires us to find the associated initial horizontal displacement through the continuity equation (43). The 4 dimensionless profiles studied by Carrier et al., and later by Kanoglu are combinations of exponentials and are given in the Eulerian frame of reference, i.e. we first have two Gaussian profiles

$$\eta_G(x,0) = H_1 exp(-c_1(x-x_1)^2) \tag{51}$$

such that $\eta_{G^+}(x,0) = \eta_G(x,0)$ is a positive Gaussian wave and $\eta_{G^-}(x,0) = -\eta_{G^+}(x,0)$ its opposite counterpart . And then, we have two different leading depression N-waves (LDN) profiles which take a form similar to:

$$\eta_N(x,0) = H_1 exp(-c_1(x-x_1)^2) - H_2 exp(-c_2(x-x_2)^2) \tag{52}$$

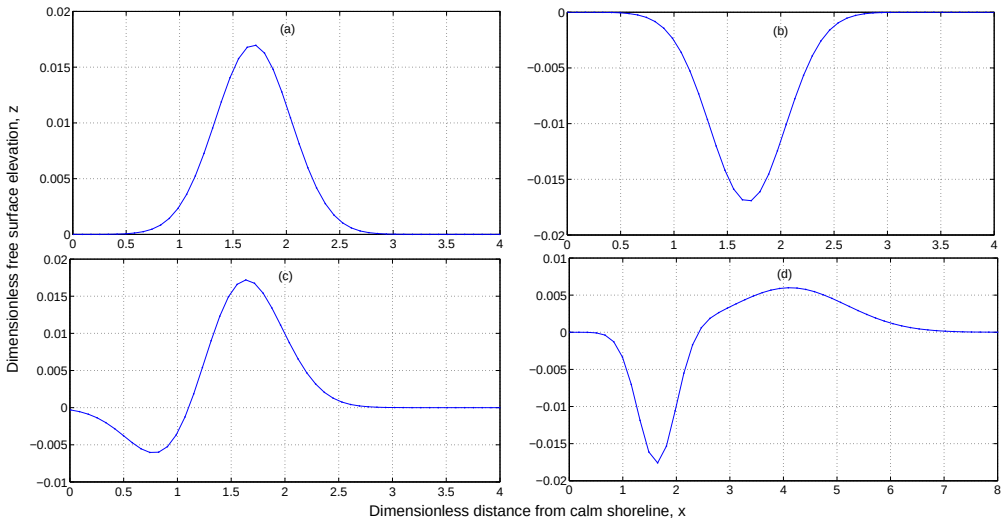

Figure 6: Carrier's four initial waveforms. Figure (a) represents the positive Gaussian with $H_1 = 0.017, c_1 = 4.0, x_1 = 1.69$, (b) its negative counterpart with $H_1 = 0.017, c_1 = 4.0, x_1 = 1.69$, (c) is the first leading depression N-waves form, i.e. $H_1 = 0.02, c_1 = 3.5, x_1 = 1.5625, H_2 = 0.01, c_2 = 3.5, x_2 = 1.0$ and (d) the second leading depression N-waves form with $H_1 = 0.006, c_1 = 0.4444, x_1 = 4.1209, H_2 = 0.018, c_2 = 4.0, x_2 = 1.6384$.

These wave forms are given in an Eulerian framework and their Lagrangian equivalent have to be found. To sum up the procedure, we first solve the continuity equation (43) for $X(a)$ at time $t = 0$, and then get $Z(a, 0)$ through $Z(a, 0) = \eta(x, 0) = \eta(a + X(a, 0), 0)$. As we integrate (43), a boundary condition has to be enforced somewhere. No better choice than setting $X = 0$ for the closest node to the shore was apparent and small discrepancies at the earliest times of the simulation could be observed as this boundary condition is not exact. Once again, the non-dimensionalization is performed using $L = 1m$ for all horizontal variables and $H = L\alpha$ for the vertical direction. As mentioned earlier, time is normalized by $\frac{\sqrt{gH}}{L}$ such that the equations of motion are independent of the slope (i.e. $\beta = 1$).

3.4.3 Results and discussion

	Positive Gaussian	Negative Gaussian	LD N-Waves form 1	LD N-Waves form 2
Parameters	$H = 0.0170$	$H = 0.0170$	$H_1 = 0.02$ $H_2 = 0.01$	$H_1 = 0.006$ $H_2 = 0.018$
Maximum runup	0.0467 (0.0470)	0.0263 (0.0268)	0.0575 (0.0583)	0.0322 (0.0328)
Maximum rundown	-0.0276 (-0.0268)	-0.0474 (-0.0470)	-0.0240 (-0.0235)	-0.0484 (-0.0484)
Maximum shoreward velocity	-0.0933 (-0.103)	-0.201 (-0.213)	-0.0152 (-0.0153)	0.106 (0.0373)
Occurring location	-0.0258 (-0.0259)	0.0365 (0.0333)	-0.0153 (-0.0167)	0.0373 (0.0371)
Maximum seaward velocity	0.219 (0.213)	0.106 (0.103)	0.232 (0.226)	-0.215 (-0.225)
Occurring location	0.0142 (0.0122)	0.0367 (0.0365)	0.00872 (0.00666)	0.0376 (0.0351)

Table 1: Comparison between the two-dimensional analytical results derived by Carrier et al. [9] and our nonlinear simulations for the runup/rundown of long-waves over a constant-slope seabed. The values found by Carrier et al. are given in between parenthesis.

All the predictions presented in this table are converged results up to a point where the code blows up as we try to refine too much the spatial grid. Indeed, if the referent particles are already very close, they may get too close as they move horizontally in time for the finite-difference techniques to work. We believe that a criterion could be obtained regarding the stability of the code. Given the length

of the physical domain, it would be based on the staggering parameter, the non-uniformity of the grid which makes it finer nearshore and the number of nodes. Fundamentally, the closer to the shore the first node is, the more likely to explode the code is. However, the stability may not be reducible to such a criterion and a lot more work is expected. Finally, the prediction of the extreme values is well acceptable when compared to Carrier et al.'s results. The small differences that can be observed are principally due to the highly unstable behavior of the code for large number of nodes nearshore[3].

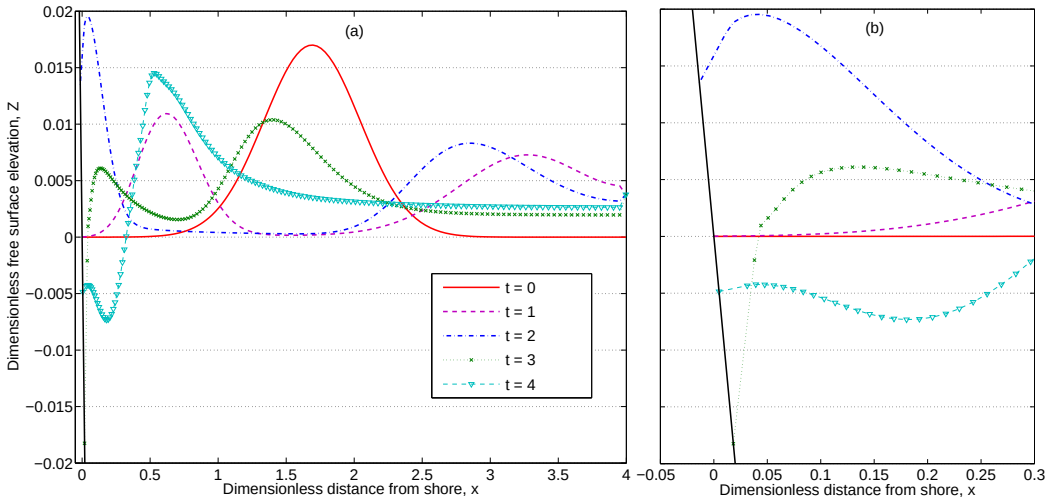

Figure 7: The evolution of a positive Gaussian wave over a constant-slope beach is observed. (a) shows that at $t = 0$ the wave starts to collapse and propagate to the right and to the left ($t = 1$), the first wave runup is then observed ($t = 2$), followed by a rundown ($t = 3$) and a second runup at $t = 4$. The thick black line on the left of the domain represents the sloping beach. (b) is a nearshore zoom of (a).

Conservation of mass and energy. The discretization in time and space of the governing equations is likely to make our simulations physically unrealistic regarding the conservation of mass and energy. Consequently, it is important to check that no mass nor energy is added or taken out of the fluid domain. To verify this we duplicate the experiments conducted for the second leading depression N-wave form presented above and close the domain. In other words, at $a = 10$ we

[3]These observations question the smoothness of the analytical solution derived by Carrier et al.; and a thorough investigation may be required to fully understand the regularity of the solutions as the domain over which the partial differential equations are solved is extended nearshore.

impose a wall boundary condition (i.e. $X_t = X_{tt} = 0$). We expect the mass or volume and the energy to be conserved since the flow is considered incompressible and inviscid. The simulations showed that the change of fluid volume relatively to the initially displaced volume is really small ($\sim 10^{-10}\%$) even for very few points ($l_a = 101$, see figure (8.a)). This allows us to conclude that mass is really well conserved in our simulations. To verify the conservation of energy we compare the potential and kinetic wave energy at all time (i.e. we subtract the potential energy of the referent calm fluid domain) with the potential wave energy of the initial deformation. We observed large relative differences ($\sim 100\%$) for very few points (i.e. $l_a = 101$, see figure (8.b)); but these variations continuously decrease as the number of nodes increases such that no more than $\sim 1\%$ of the initial wave energy fluctuates in an out of the fluid domain when we take 801 spatial points or more (figure (8.c)). Specifically, the energy is really well conserved up to the point when the wave reaches the shore and a large runup or drawdown occurs.

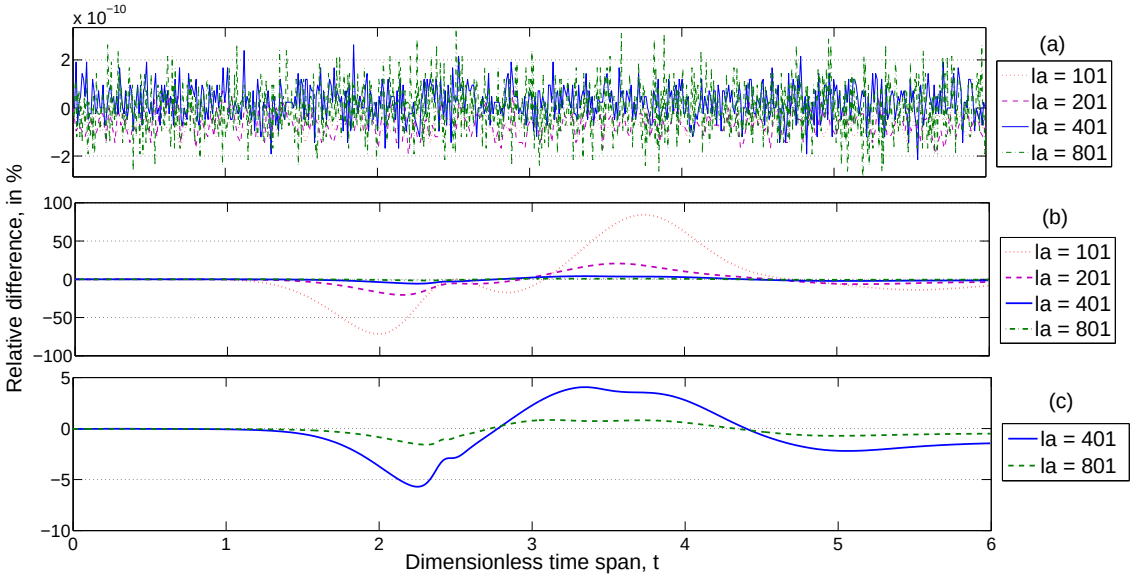

Figure 8: (a) shows the relative variations of volume or mass to the initial displaced volume or mass. The pattern is much like a noise signal. (b) and (c) show the relative differences of wave energy over time to the initial wave energy. For very few points, that is $la = 101$, the difference gets above $\sim 50\%$ when the runup and rundown phenomena occur. However, these variations decrease uniformly as the number of nodes increases. The setup and initial value problem is the one corresponding to the second leading depression wave experiment (presented above).

4 Validation of the three-dimensional linear model

Here we address the effect of including a second horizontal dimension in our simulations. The numerical procedure is not presented as it rigorously follows the logic embedded in the two-dimensional model.

The three-dimensional validation is a crucial step, yet hard to fulfill. Very few analyses of three-dimensional long-waves have been published as mentioned by Sammarco and Renzi [8]. Lynett et al. started with a two-dimensional analysis of landslides' generated waves in 2002 [13] and 2003 [14] before taking into account the third dimension in 2005 [15]. They found that the highest runup and lowest rundown along the shoreline cannot be observed with a two-dimensional model. Most of their observations can be found in our own simulations. However, their formulation is less restrictive than ours regarding the long-waves assumption and will need subsequent validations before serving as a benchmark test. Therefore, we chose to validate our linear numerical model against the results presented by Sammarco and Renzi in 2008 [8]. They derived a linear analytical solution in the Eulerian framework for the propagation and runup of long-waves generated by a landslide. Their assumptions and ours are similar, thus allow meaningful comparisons.

We first describe the seabed motion that mimics the moving landslide. Secondly, the initial value problem is carefully addressed. Finally, our linear three-dimensional formulation is validated against their closed form solution and we discuss and compare the snapshots they presented with ours.

4.1 Seabed perturbation and normalization

The numerical experiment is an initial value problem together with a moving seabed. At time $t = 0$, the calm water surface is forced to move as a landslide runs down a uniformly inclined beach of slope α. The profile of the bottom is given by $h(x, y, t) = h(x) - f(x, y, t)$ where f is the perturbation. The dimensional equation governing the motion of the free surface and considered by Sammarco and Renzi is as follows

$$\zeta_{tt} - gs\nabla.(x\nabla\zeta) = f_{tt} \tag{53}$$

where s is the beach slope and ζ the free surface elevation. The normalization of this equation made them consider

$$x\zeta_{xx} + \zeta + x\zeta_{yy} = \zeta_{tt} - f_{tt} \tag{54}$$

where the variables and coordinates are now dimensionless such that $f(x, y, t) = \exp(-(x - t)^2)\exp(-4y^2)$ as both the free surface elevation and the perturbation have been scaled by the vertical thickness of the landslide. It should be noticed

that the landslide is slightly longer (in the offshore direction) than wide (in the shoreline direction), is symmetric with respect to the x-axis and its dimensionless velocity is set to 1.

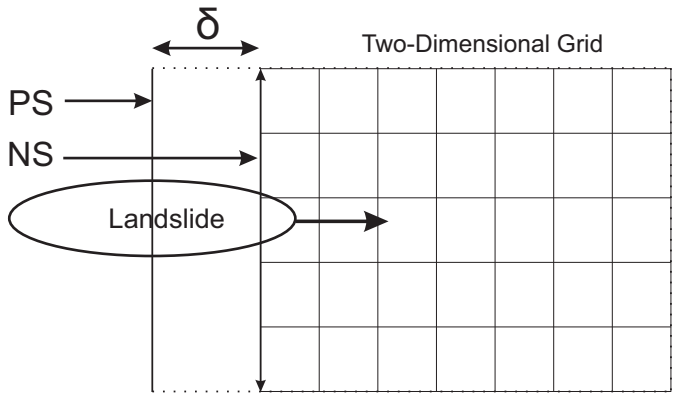

Figure 9: This is the geometry of the three-dimensional problem. The physical and staggered shorelines (PS, NS) are on the left-hand-side (y-direction). δ is the distance between the two in the referent configuration. All other frontiers of the domain are open boundaries. The landslide is set to move away from the shoreline (in the x-direction) at a constant speed.

It is remarkable that equation (54) is independent of the slope angle and only invokes the perturbation function through its acceleration f_{tt}. The normalization of the Lagrangian three-dimensional linear equations (32) (33) (34) is performed using $L = 1\ m$ and $H = L\alpha$ for the horizontal and vertical variables respectively. The dimensional time is normalized by $\frac{L}{\sqrt{gH}}$. The water depth is consistently scaled by H and takes the following dimensionless form

$$h(x, y, t) = x - T \exp(-(x - t)^2) \exp(-4y^2) \tag{55}$$

where T is the dimensionless thickness of the landslide. The non-dimensionalization of the governing equations shows that the slope angle α is not a relevant parameter in our simulation. Note that the complete water depth function, that is the straight slope and the perturbation, is invoked twice in the Lagrangian continuity equation (34). Therefore the value of T matters in the Lagrangian simulations contrarily to what would be predicted by the Eulerian equivalent (54). However, the two-dimensional equivalent of this equation and the associated derivation can be found in the work of Tuck and Hwang [19]. Their authors clearly show that the resulting equation has a convenient form because the water depth function is approximated by the constant-slope seabed when there is no time-derivative to apply. This approximation explains why the bottom perturbation is only found on the right-hand-side of equation (54) or (2.1) in Sammarco and Renzi [8] and

allows a convenient scaling to get rid of T. This difference in the two formulations is somehow attenuated by the infinitely thin landslide assumption. This condition simply forces $T\alpha \ll 1$ and no visual differences could be observed as we ran our simulations for different values of T in that range. Note that we had to multiply by $\frac{1}{T}$ the dimensionless free surface elevation Z predicted by our numerical simulations to obtain a dimensionless waves height comparable with what Sammarco and Renzi presented [8].

4.2 Initial value problem for a three-dimensional landslide

The transfer of the Eulerian initial values to the Lagrangian framework is probably the trickiest part as one tries to compare the two different approaches. In particular, the calm water free surface with zero initial velocity proposed by Sammarco and Renzi is somehow deceptive. Indeed, the initial value problem $\eta_t(x, y, 0) = 0$ is not always equivalent to $Z_t(a, b, 0) = X_t(a, b, 0) = Y_t(a, b, 0) = 0$. While the calm water free surface condition can actually be enforced by having no initial displacements[4], i.e. $\eta(x, y, 0) = 0 \leftrightarrow Z(a, b, 0) = X(a, b, 0) = Y(a, b, 0) = 0$, the initial velocities cannot be uniformly zero if the seabed deforms at time $t = 0$. Let us now recall the three-dimensional linear continuity equation derived in preceding sections.

$$Z(a, b, 0, t) = h(a, b, 0)(1 - X_a - Y_b) - h(X + a, Y + b, t) \tag{56}$$

This equation involves both Lagrangian and Eulerian variables as h is a function of the instantaneous location, on the contrary of X, Y, Z, which only depend on the referent positions and time t. One has to remember that the time derivative of $Z(a, b, 0, t)$ is a material derivative. As a consequence, assuming $X = Y = 0$ at $t = 0$, we seek $X_t(a, b, 0), Y_t(a, b, 0)$ satisfying

$$Z_t(a, b, 0, t) = h(a, b, 0)(-X_{a,t} - Y_{b,t}) - h_t(a, b, 0) - X_t h_a(a, b, 0) - Y_t h_b(a, b, 0) \tag{57}$$

This equation is a linear first order partial differential equation on both X_t and Y_t. There is only one boundary condition for the two-dimensional velocity vector on the shoreline. Therefore, the integration of (56) does not have a unique solution. Numerically solving (56) is surprisingly tedious and we assumed that $Y_t = 0$ could be set to zero as Sammarco and Renzi observed that the water was initially pushed forward at the earliest time of their analyses. We do not deal with the boundary condition on the shoreline since the particles on the shore are not part of our grid. Indeed, we recall that in the referent configuration, the closest points to

[4] As a general remark, whenever the free surface is supposed to be initially still, the initial situation can match the referent configuration and the Lagrangian displacements should be set to zero. This intuitive solution is not unique but perfectly satisfies the continuity equation.

the shoreline that are being updated in our code are moved away by a distance equal to δ for stability reasons. Hence, we use (58) to find X_t on this staggered shoreline, and (56) is then integrated to obtain it everywhere else.

$$Z_t(a,b,0,t) = 0 = -h_t(a,b,0) - X_t h_a(a,b,0) \tag{58}$$

Note that we take the physical domain large enough (e.g. $a_{max} = b_{max} = 16$) so that the initial horizontal displacements induced by the localized disturbance are approximately zeros at the offshore boundaries, i.e. $X(a_{max}, b, 0) = X(a, b_{max}) \approx 0 \forall (a,b)$. This large domain also allows us to consider that reflections coming from these offshore boundaries do not have time to travel all the way back to the point where we study the runup phenomenon (i.e. $(a,b) \in [0,4]^2$) for the time span considered (i.e. $t \in [0,7]$). Ideally, we would like to enforce an open boundary conditions but because of the difficulty of its implementation we simply extended our computational domain to an ideal size[5]. Finally, the initial value integration is surely arguable and the transfer of the initial value problem from one framework to another should be standardized in the near future. However, as showed in the following section, this simplification yielded acceptable results to be compared with those of Sammarco and Renzi [8].

4.3 Results and discussions

Here we validate our formulation and its numerical implementation against the closed form solution of (54) derived by Sammarco and Renzi in 2008:

$$\zeta(x,y,t) = \frac{2}{pi} \sum_{n=0}^{\infty} \int_0^{\infty} \exp(-kx) L_n(2kx) T_n(k,t) \cos(ky) dk \tag{59}$$

The functions L_n are the Laguerre polynoms and T_n is given by equation (2.16) in [8] and is a function of the variable of integration k and time t. The index n is referred to as the mode number such that $n = 0$ is the fundamental mode, $n = 1$ the first mode, ... etc.

[5]By which we mean that a larger domain induces no difference for the runup close to the initial position of the landslide whereas a smaller domain produces observable differences.

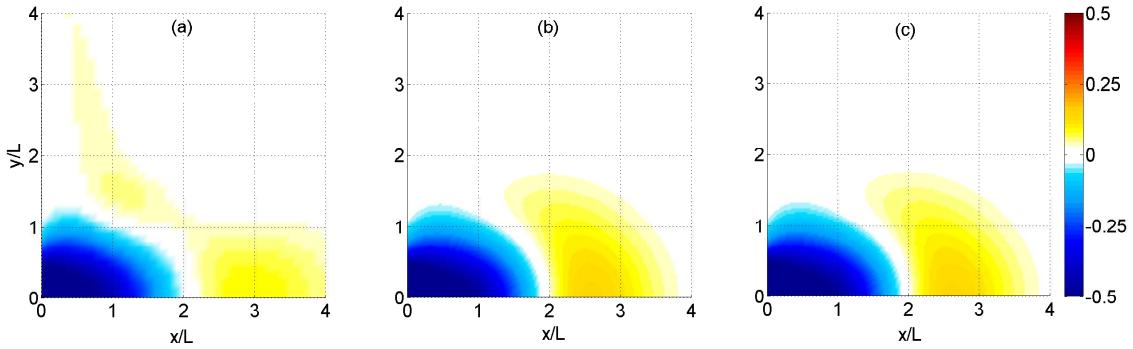

Figure 10: Spatial snapshots at time $t = 1.5$ of the (a) theoretical solution with 6 modes considered (b) simulation of the Eulerian equation and (c) simulation of the Lagrangian set of equations. The numerical simulations were both run with a uniform spatial step of 0.025 in the two horizontal directions and were converged in terms of both time and spatial steps. They are qualitatively identical but largely differ from the 6 modes analytical solution derived by Sammarco and Renzi.

The integrals in (59) tend rapidly to 0 as n increases. Thus Sammarco and Renzi displayed snapshots of the free surface for a limited number of 6 modes[6]. It turns out that the 6 modes solution is not really well converged and present wave patterns that are absent from the simulations of both the Eulerian (54) and Lagrangian (32) (33) (30) equations. The most striking example is presented in figure (10) where the analytical 6 modes solution is compared with the numerical simulations of the Eulerian[7] and Lagrangian equations at time $t = 1.5$. Fortunately, it can be seen in figure (11) that the closed form solution they derived eventually tend to the numerical solution as the number of modes increases.

[6]Figure 5 in [8].

[7]We discretized the Eulerian equation and simulated the landslide's generated waves with a basic finite-difference technique only to verify that it was coherent with our Lagrangian simulations.

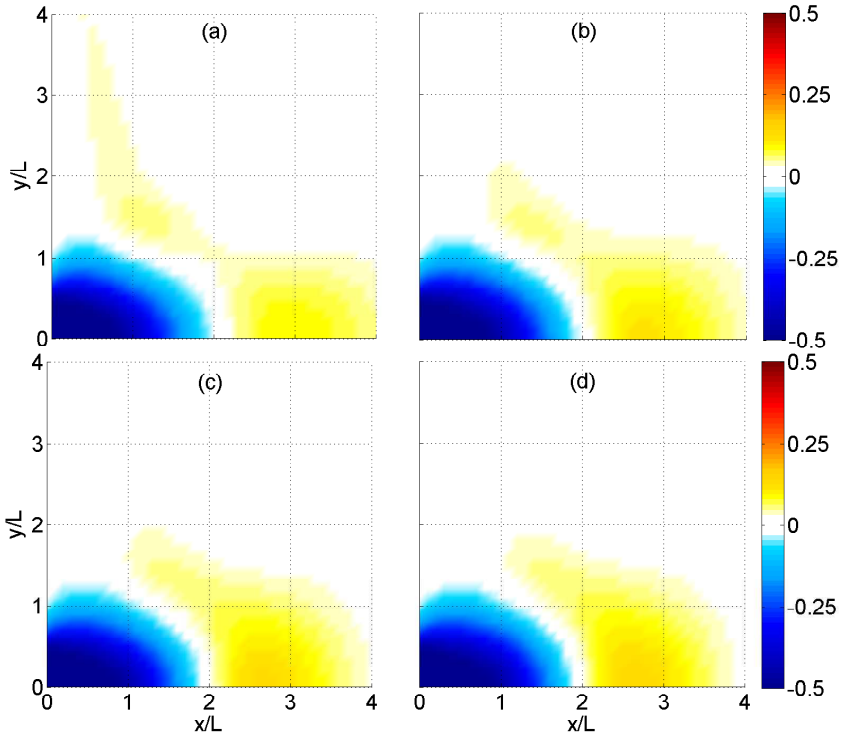

Figure 11: Spatial snapshots at time $t = 1.5$ of the theoretical solution with (a) 6 modes (b) 9 modes (c) 12 modes and (d) 17 modes considered. The analytical solution tends to the numerical predictions presented in the previous figure. Note that the sharp edges are due to the low resolution of the plots.

Finally, we present the numerical solutions at time $t = 0.5, 1.5, 4.5, 7$ of the Lagrangian equations in figure (12). They look like the 6 modes solutions issued by Sammarco and Renzi but some major differences (e.g. upper left corner of the predictions at time $t = 1.5$ or lower right corner at $t = 7.0$) are observable and indicates that more than 6 modes should be taken into account for a physical interpretations of the analytical solution. Nonetheless, most of their comments are similar to what can be inferred from figure (12). Specifically, water is initially pushed forward (figure (12.a)) and a depression wave, landward of the landslide's peak occurs shortly after (figure (12.b)). As time goes by, the landslide dives into deeper water such that the generated continuous elevation wave slowly vanishes and edge waves become dominants along the shoreline direction (figure (12.c) and (12.d)). All these effects have already been observed by Lynett and Liu [15] and show that the consideration of a three-dimensional fluid domain gives physical insights on waves' propagation that could not be extrapolated from two-dimensional studies.

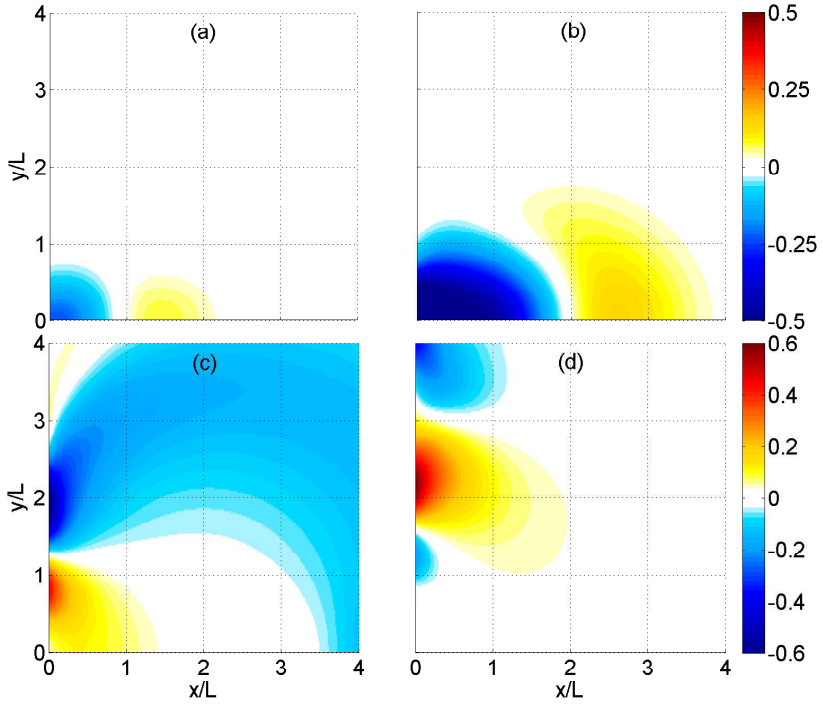

Figure 12: Spatial snapshots at four different times of the free surface elevation with a zero initial vertical displacement and velocity. The simulation is based on the three-dimensional Lagrangian linear model. (a) t = 0.5, (b) t = 1.5, (c) t = 4.5, (d) t = 7.0. These predictions are obtained for non-uniform grids with 1024 and 512 nodes in the landslide direction of propagation and transverse direction respectively. Note that the computational domain is 4 times longer and wider than what is displayed to avoid reflections from the offshore boundaries.

5 Conclusions

We presented two- and three-dimensional numerical simulations of linear and nonlinear long-waves in a Lagrangian framework. The motivations for this work were numerous.

As said in the introduction, very few analyses of shallow-water waves have taken advantage of the Lagrangian point of view. Since the ocean can be seen as a continuous medium, following fluid particles is inconvenient in many practical applications. However, a few situations may be perfectly fitting for a Lagrangian approach. For instance, the runup of nonlinear long-waves, which can displace the shoreline over large distances inland, may be more easily studied in the Lagrangian than in the Eulerian framework.

Shuto [5], Shuto and Nobuo [12] and Fujima [6] contributed to the development of the Lagrangian approach, but many more supported and further enhanced the findings of Carrier and Greenspan [7] in the Eulerian framework, thus leaving space for new works in Lagrangian. Under strong restrictions, analytical predictions of extreme runup for different initial waveforms have been successfully obtained in the past in the two different frame of reference. Fortunately, the condition of a constant-slope seabed assumed by Carrier and Greenspan in 1958 was somehow relaxed by the work of Synolakis [10], as his formulation allows the analysis of waves running up and down a combination of constant-depth and constant-slope seabeds. However, their derivations remain valid for very specific initial profiles only. This makes their predictions potentially nonphysical if their initial waveform does not resemble well enough real-life waves. Specifically, the solitary wave was thought for many years to be a good approximation of tsunamis, but Madsen et al. [20] denied this paradigm and have advocated the use of field measurements to initialize both experiments and computations if physical interpretations of geophysical tsunamis are to be drawn. Therefore, all analytical solutions that have been derived under the assumption of solitary wave cannot predict accurately geophysical tsunamis' extreme runup and drawdown.

Numerical models are expected to provide further insights because they do not depend on initial waveforms and can handle arbitrary seafloors. In that respect, we implemented a numerical scheme that can simulate the propagation and runup of two- and three-dimensional long-waves over any type of seabed. Incompressibility, vertical irrotationality and inviscid flow were assumed while nonlinearity was included in the model. The two- and three-dimensional numerical models were successfully validated against existing analytical results, though the scheme needs improvements. In particular: offshore boundaries are not dealt with such that outgoing waves leave the computational domain; forward-finite-difference techniques may not be physically satisfactory at the shoreline; and, the procedure to transfer the initial-value problem from the Eulerian to the Lagrangian framework should

be standardized.

Finally, our objectives are not to overthrow existing softwares used for tsunamis' forecasting but rather to rapidly be able to research on revolutionary topics. For instance, the Method of Splitting Tsunami (MOST) developed by Titov and Synolakis is the standard model used by national institutions for tsunamis' propagation and inundation forecasting and certainly deserves all the credits it received. However, such a program may not be appropriate for research purposes. Therefore, we expect to extensively use our code to investigate new practical applications. In particular, we hope to work on new tsunami mitigation techniques.

References

[1] F. Ursell. The long-wave paradox in the theory of gravity waves. *Mathematical Proceedings of the Cambridge Philosophical Society*, 49(04):685, October 1953.

[2] J. V. Wehausen. Use of Lagrangian Coordinates for Ship Wave Resistance. *Journal of Ship Research*, 13(1), 1969.

[3] M. S. Longuet-Higgins and E. D. Cokelet. The Deformation of Steep Surface Waves on Water. I. A Numerical Method of Computation. *Proceedings of the Royal Society A: Mathematical, Physical and Engineering Sciences*, 350(1660):1–26, July 1976.

[4] R. W. Yeung. Numerical Methods in Free-Surface Flows. *Annual Review of Fluid Mechanics*, 14(1):395–442, January 1982.

[5] N. Shuto. Run-up of long waves on a sloping beach. *Coastal Engineering in Japan*, 10, 1967.

[6] K. Fujima. Tsunami Runup in Lagrangian Description. In Anjan Kundu, editor, *Tsunami and Nonlinear Waves*, pages pp 191–207. Springer Berlin Heidelberg, 2007.

[7] G. F. Carrier and H. P. Greenspan. Water waves of finite amplitude on a sloping beach. *Journal of Fluid Mechanics*, 4(01):97, March 1958.

[8] P. Sammarco and E. Renzi. Landslide tsunamis propagating along a plane beach. *Journal of Fluid Mechanics*, 598:107–119, February 2008.

[9] G. F. Carrier, T. T. Wu, and H. Yeh. Tsunami run-up and draw-down on a plane beach. *Journal of Fluid Mechanics*, 475(March 2002):79–99, February 2003.

[10] C. E. Synolakis. The runup of solitary waves. *Journal of Fluid Mechanics*, 185(-1):523, April 1987.

[11] S. Tadepalli and C. E. Synolakis. The Run-Up of N-Waves on Sloping Beaches. *Proceedings of the Royal Society A: Mathematical, Physical and Engineering Sciences*, 445(1923):99–112, April 1994.

[12] N. Shuto and T. Goto. Numerical simulation of tsunami run-up. *Coastal Engineering in Japan*, 21, 1978.

[13] P. Lynett and P. L. F. Liu. A numerical study of submarine-landslide-generated waves and run-up. *Proceedings of the Royal Society A: Mathematical, Physical and Engineering Sciences*, 458(2028):2885–2910, December 2002.

[14] P. L.-F. Liu, P. Lynett, and C. E. Synolakis. Analytical solutions for forced long waves on a sloping beach. *Journal of Fluid Mechanics*, 478:101–109, March 2003.

[15] P. Lynett. A numerical study of the run-up generated by three-dimensional landslides. *Journal of Geophysical Research*, 110(C3):C03006, 2005.

[16] J. A. Zelt. The run-up of nonbreaking and breaking solitary waves. *Coastal Engineering*, 15(3):205–246, June 1991.

[17] J. A. Zelt and F. Raichlen. A Lagrangian model for wave-induced harbour oscillations. *Journal of Fluid Mechanics*, 213:203–225, 1990.

[18] U. Kânolu. Nonlinear evolution and runuprundown of long waves over a sloping beach. *Journal of Fluid Mechanics*, 513:363–372, August 2004.

[19] E. O. Tuck and L. S. Hwang. Long wave generation on a sloping beach. *Journal of Fluid Mechanics*, 51(03):449, March 1972.

[20] P. A. Madsen, D. R. Fuhrman, and H. A. Schäffer. On the solitary wave paradigm for tsunamis. *Journal of Geophysical Research*, 113(C12):C12012, December 2008.